Graft Copolymers with Regularly Spaced, Tetrafunctional Branch Points: Morphology and Grain Structure

Frederick L. Beyer,[†] Samuel P. Gido,[*,†] Christine Büschl,[†] Hermis Iatrou,[‡,#] David Uhrig,[‡] Jimmy W. Mays,[‡] Mei Ying Chang,[§] Bruce A. Garetz,[§] Nitash P. Balsara,[§] Nora Beck Tan,[⊥] and Nikos Hadjichristidis[#]

Department of Polymer Science & Engineering, University of Massachusetts, Amherst, Amherst, Massachusetts 01003; Department of Chemistry, University of Alabama at Birmingham, Birmingham, Alabama 35294; Departments of Chemical Engineering, Chemistry, Materials Science, and Electrical Engineering, Polytechnic University, Six Metrotech Center, Brooklyn, New York 11201; U. S. Army Research Laboratory, Aberdeen Proving Grounds, Maryland 21005; and Department of Chemistry, University of Athens, Panepistimiopolis Zografou 15771, Athens, Greece

Received July 13, 1999; Revised Manuscript Received January 21, 2000

ABSTRACT: An investigation of the morphological behavior of a series of graft copolymers having multiple regularly spaced, tetrafunctional branch points has been carried out. The behavior of these materials, comprised of polyisoprene backbones with two polystyrene arms grafted to the backbone at each branch point, is shown to be effectively modeled by considering the behavior of smaller, architectural subunits based on the local environment of each junction point (constituting block copolymer). Morphological behavior was characterized using TEM and SAXS. Well-ordered cylindrical and lamellar morphologies were observed. Several samples appear to form cylindrical domains in disordered arrangements. Samples predicted to form spheres form instead a microphase-separated "mesh" morphology. Lamellar grain size and shape were also investigated, and lamellar grain orientation correlation lengths were determined. These measurements show a decrease in grain size with increasing number of branch points per molecule. They also indicate that the grains formed are anisotropic in shape.

Introduction

Molecular architecture has been demonstrated to be an important factor in the morphological behavior of block copolymers. Systematic studies of the relationship between molecular architecture and morphology have been largely restricted to diblock and triblock copolymers due to the unavailability of model graft copolymer materials with precisely controlled architectures. Common methods of producing graft copolymers often yield materials with heterogeneous, ill-defined architectures. As illustrated in Figure 1a, characteristics of such materials included polydisperse backbones and arms, irregular placement of branch points, and variation in the number of branch points per molecule.[1]

New synthetic techniques allow synthesis of graft block copolymers having well-defined molecular architectures.[2,3] These techniques provide precise control over backbone molecular weight, arm molecular weight, arm polydispersity, the placement of the branch points along the backbone, and the number of arms grafted to each branch point. Molecules with specific, incremental backbone lengths are produced, allowing multiple grafts with well-defined architectures to be isolated and characterized.

An empirical framework for predicting and interpreting the morphological behavior of block copolymers with complex architectures has been developed.[4−7] This framework, the *constituting block copolymer hypothesis*, proposes that the morphological behavior of a graft copolymer with a complex architecture is governed by the behavior of smaller block copolymer units (the constituting block copolymers) associated with each junction point. Existing theories for miktoarm stars,[8,9] or conformationally asymmetric linear diblocks,[10,11] are used to predict the behavior of the constituting block copolymer, which is then applied to the overall multigraft architecture. The constituting block copolymer hypothesis for strongly segregated graft copolymers is reminiscent of the calculations of Benoit and Hadziioannou for graft copolymers in the homogeneous state

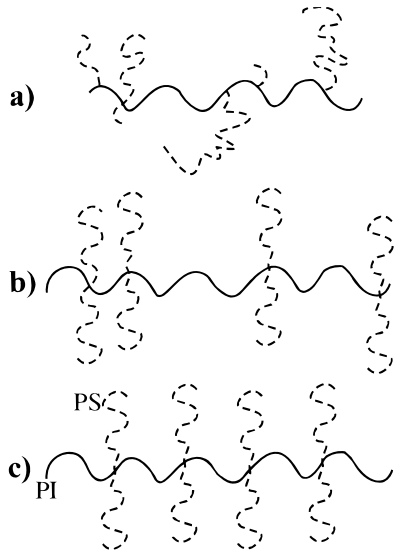

Figure 1. Illustrations of (a) a multigraft having a heterogeneous, ill-defined architecture, (b) a multigraft with randomly placed, tetrafunctional branch points, and (c) a multigraft of PI and PS with regularly placed, tetrafunctional branch points.

[†] University of Massachusetts.
[‡] University of Alabama at Birmingham.
[§] Polytechnic University.
[⊥] U. S. Army Research Laboratory.
[#] University of Athens.
* To whom all correspondence should be addressed.

10.1021/ma991141s CCC: $19.00
Published on Web 03/02/2000

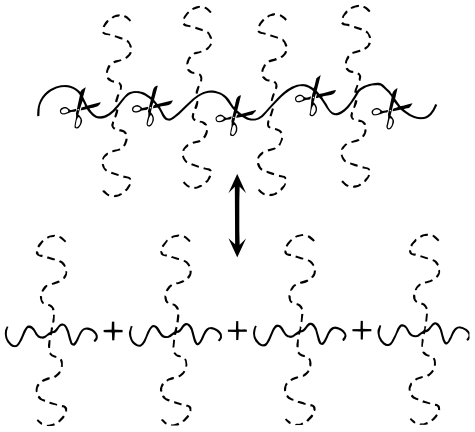

Figure 2. Illustration of the constituting block copolymer hypothesis as applied to a regular multigraft having tetrafunctional branch points. Imaginary division of the tetrafunctional regular multigraft produces identical A_2B_2 miktoarm star block copolymers.

and at the spinodal.[12] They found that the scattering profiles for multigraft copolymers as well as the spinodal curves were relatively insensitive to the total number of constituting units, approaching a limiting value at high numbers of these units. Additionally, they found that the relevant value of χN for controlling phase behavior was that of the constituting unit rather than of the whole graft copolymer. A similar result was found by Balazs and co-workers when considering the order−disorder transition behavior of comb copolymers.[13]

Recently we studied the morphological behavior of multiple-graft block copolymers with monodisperse polybutadiene (PB) backbones, monodisperse polystyrene (PS) arms, and branch points located randomly along the PB backbone.[7] The average number of branch points per molecule was controlled as described by Xenidou and Hadjichristidis.[2] Each branch point was either trifunctional, allowing one arm of PS to be grafted to the PB backbone, or tetrafunctional, allowing two PS arms to be grafted to the PB backbone at the same point. The tetrafunctional random multigraft illustrated in Figure 1b represents a moderate level of architectural heterogeneity, intermediate between the precisely defined architectures of the molecules examined in this work and the case of common multiple-graft architectures with much more heterogeneous molecular architectures. It was observed that while the constituting block copolymer hypothesis, based on the average environment around each junction point, correctly predicted domain shape preferences, only lamellar morphologies formed with long-range order. When nonlamellar morphologies were predicted, the samples were observed to form microphase-separated morphologies, characterized by form factor scattering indicating the formation of specific domain shapes (spheres or cylinders) that were not, however, ordered on lattices. These preferred domain shapes agreed with the predictions made using the constituting block copolymer hypothesis.

In the present study, the morphological behavior of a series of multiple-graft block copolymers with regularly spaced branch points is characterized. These multigrafts, illustrated in Figure 1c, have monodisperse polyisoprene (PI) backbones, monodisperse PS arms, and tetrafunctional branch points. As shown in Figure 2, the molecular architecture of these materials may be thought of as serial combinations of I_2S_2 miktoarm stars. The synthesis utilizes a polycondensation reaction that connects the constituting block copolymer I_2S_2 units. As discussed in the Experimental Section, this approach puts PI blocks on the two ends of each molecule which are the same length as all the other PI connectors. As illustrated in Figure 2, these end PI blocks must also be imagined to be cut in the middle in order to give a uniform structure for all the constituting I_2S_2 units. The ends of each of these outer PI blocks are thus neglected in the definition of the constituting unit. The inaccuracy resulting from this approximation becomes less severe as the number of junction points per molecule increases.

Several issues are considered. First, the effectiveness of the constituting block copolymer hypothesis for the regular multigraft block copolymer architecture is evaluated. Second, the polycondensation technique used to produce the regular multigraft copolymers produces a distribution of molecular weights but with all molecules having the same exact composition because they are all based on the same constituting unit. This allows an important self-consistency check to the constituting block copolymer hypothesis. Specifically, different average molecular weight fractions based on the same constituting block copolymer can be isolated and should form the same morphology. It is expected that as molecular weight (number of junction points per molecule) increases, long-range order will decrease but the domain shape should be conserved. Thus, the internal consistency of the constituting block copolymer hypothesis can be evaluated even if the samples at a particular volume fraction are found to disagree with predictions of theories such as that of Milner.[8]

The decrease in long-range order with increasing numbers of junction points per molecule is investigated quantitatively for a series of three regular multigraft fractions all based on the same constituting block copolymer unit and all forming lamellar morphologies. This is achieved by measuring the average grain size by analysis of TEM images of the morphologies of these materials. Additionally, the grain shape anisotropy in these samples is measured.

Experimental Section

Synthesis. A series of multigrafts having regularly spaced, tetrafunctional branch points were synthesized as described by Iatrou, Mays, and Hadjichristidis.[3] The synthesis of these materials is a multiple-step process beginning with the polymerization of very low polydispersity PI dianions by living anionic polymerization. PS arms are also polymerized separately by living anionic polymerization. The molecular characteristics of the component PI blocks and PS arms for each composition are given in detail in Table 1. A macrocoupling agent is then created by joining two PS arms with a tetrafunctional chlorosilane coupling agent, leaving two functionalized sites on the silicon. In the final reaction, PI dianions and PS macrocoupling agents are reacted to form multigrafts with regularly spaced branch points, where the PI blocks form a backbone with two PS arms at each branch point. Stoichiometry is adjusted to ensure that the regular multigraft has PI blocks at both ends. The polycondensation nature of this final step produces a most-probable, Flory−Schultz distribution of multigraft molecular weights, equivalent to a distribution in number of branch points and in number of constituting block copolymer units per molecule. Each species has nearly identical volume fractions of PS and has the same constituting block copolymer. Through solvent−nonsolvent fractionation, two or three average molecular weight fractions are obtained from each overall polycondensation product. Four compositions were examined, with 10 samples studied in all, as indicated in Table 2.

Molecular Characterization. The molecular characteristics of the component blocks and the regular multigrafts were

Table 1. Molecular Characteristics of the PI and PS Connectors and Arms Comprising the Regular Multigrafts

	PS branch					PI connector		
	SEC		MALDI		MO	SEC		MO
sample	M_n (g/mol)	PDI	M_n (g/mol)	PDI	M_n (g/mol)	M_n (g/mol)	PDI	M_n (g/mol)
MG-4-*x*-9	6 500	1.05	6 790	1.029		100 600	1.17	91 600
MG-4-*x*-21	13 400	1.03	14 070	1.014		82 800	1.15	72 700
MG-4-*x*-36	23 900	1.03	25 500	1.005	28 800	60 300	1.22	61 800
MG-4-*x*-67	29 100	1.02	31 900	1.009	34 400	26 100	1.35	27 400

Table 2. Molecular Characteristics of the Regular Multigraft Block Copolymers with Tetrafunctional Branch Points

sample	wt % PS (NMR)	wt % PS (SEC-UV)	vol % PS[a]	total M_w (SEC-MALLS, kg/mol)	total M_w (LALLS, kg/mol)	PDI (SEC)	M_n constituting unit (kg/mol)	no. of branch points[b]
MG-4-4-9	10.3	12.0	9.1	589	540	1.24	113.6	4.3
MG-4-8-9	10.8	11.9	9.6	994	1020	1.22	113.6	7.9
MG-4-4-21	23.6	24.9	21.3	565	600	1.29	109.6	4.4
MG-4-7-21	23.8	25.2	21.5	798	830	1.23	109.6	6.5
MG-4-9-21	23.9	25.6	21.6	1094	1170	1.26	109.6	9.2
MG-4-5-36	40.2	41.4	37.0	570	600	1.41	108.1	4.7
MG-4-9-36	39.3	41.6	36.2	983	950	1.32	108.1	8.5
MG-4-12-36	38.6	40.1	35.5	1351	1260	1.37	108.1	11.9
MG-4-10-67	69.6	70.3	66.7	827	800	1.26	84.3	9.5
MG-4-14-67	69.4	70.4	66.5	1166	1220	1.28	84.3	13.5

[a] Calculated using wt % PI from NMR, $\rho_{PI} = 0.91$ g/cm^3, and $\rho_{PS} = 1.05$ g/cm^3. [b] Number of branch points calculated as (total $M_{w(SEC-MALLS)}$ − PI connector $M_{n(SEC)}$)/(constituting block copolymer M_n).

determined using a variety of techniques. Size-exclusion chromatography (SEC) was performed for solutions in tetrahydrofuran (THF) at 30 °C using a Waters model 510 pump, Waters model 410 differential refractometer, and Ultrastyragel columns with a continuous porosity range from 10^6 to 10^3 Å. Ultraviolet size-exclusion chromatography (SEC-UV) was performed on solutions in THF at 30 °C and a flow rate of 1 mL/min using a Waters Alliance separations module 2690 and a Waters photodiode array detector 996. Multiangle laser light scattering size-exclusion chromatography (SEC-MALLS) was performed using a Waters Alliance separations module 2690, a Waters refractive index detector 2410, and a Wyatt Technology Dawn DSP laser photometer with solutions in THF at 30 °C with a flow rate of 1 mL/min. Low-angle laser light scattering (LALLS), used to obtain an independent measure of weight-average molecular weight, was performed on multigraft solutions in THF at 22 °C using a Chromatix KMX-6 instrument with $\lambda = 633$ nm. Membrane osmometry (MO) using a Jupiter model 231 recording membrane osmometer was conducted in toluene distilled from CaH_2. Matrix-assisted laser desorption/ionization time-of-flight mass spectroscopy (MALDI/TOF/MS) was performed in *trans*-retinoic acid with silver trifluoroacetate using a Perseptive Biosystems Voyager Elite DE instrument. Finally, nuclear magnetic resonance (NMR) was used to determine overall weight fractions of PS in each sample. The molecular characterization data are listed in Tables 1 and 2.

To describe molecular architecture, the following notation is used: MG-*f*-*n*-ϕ, where MG stands for *multigraft*, *f* describes the functionality of the branch points, *n* gives the average number of branch points per molecule in a particular fraction, and ϕ is the overall volume fraction of PS in the sample. This nomenclature differs from that used by Iatrou, Mays, and Hadjichristidis[3] but is consistent with the previous work on random multigrafts.[7]

Morphological Characterization. For multigrafts having tetrafunctional branch points, an A_2B_2 miktoarm star of PI and PS (I_2S_2) is the appropriate constituting block copolymer. The two PI arms in the constituting I_2S_2 are each $^1/_2$ the length of a single PI connector. To calculate the number of branch points per molecule in a given fraction, the average molecular weight of the fraction, less the molecular weight of one PI connector, is divided by the molecular weight of the constituting block copolymer. Even after fractionation, the samples obtained contain a distribution of molecular weights and of number of constituting units per molecule. Polydispersities for all samples are listed in Table 2. Note that the polydispersities of the fractionated samples used in this study are still broader than the polydispersities of the of the multigraft materials with random graft placement used in our previous study.[7] The previous random multigraft materials were based on grafting from a anionically synthesized, near-monodisperse polybutadiene backbone. While the overall polydispersities of the random multigraft samples were lower than in the regular multigraft samples of this study, the regular multigrafts have a very well-defined constituting block copolymer, and the random multigrafts had more dispersity in the structure associated with each junction point. The degrees of segregation, χN, are calculated for the constituting block copolymers, where χ is the Flory−Huggins parameter and N is the degree of polymerization for the constituting block copolymer. These values, listed in Table 3, place all the samples in the strong segregation limit. These χN valued are expected to accurately represent the degrees of segregation for the various multigraft copolymers.[4,14]

Morphological characterization of each sample followed established techniques for block copolymers. Solid films approximately 1 mm thick were cast from 2.5 wt % solutions in toluene, a nonpreferential solvent for PS and PI.[15] To promote the formation of equilibrium morphologies, solvent evaporation was restricted to allow approximately 8 weeks for the solidification of a bulk film. To further promote the formation of equilibrium morphologies, the samples were annealed at 120 °C under vacuum for a period of 2 weeks. These casting and annealing conditions allow a much greater period of time for self-assembly than is usual for block copolymers having simple architectures. To allow for comparison of long-range order and grain size, all samples in the study were cast and annealed together, ensuring that they experienced identical conditions. After annealing, thin sections approximately 500−1000 Å thick were prepared by ultramicrotoming the bulk films using a Leica EM-FCS microtome, equipped with a cryogenic sample chamber operated at −110 °C. The sections were stained 4 h in OsO_4 vapors for transmission electron microscopy (TEM) imaging of the structures. TEM was performed using either a JEOL 100CX TEM or a JEOL 2000FX TEM, both operated at an accelerating voltage of 100 kV.

Small-angle X-ray scattering (SAXS) experiments were performed to determine the lattice symmetries, domain shapes, and spacings of the morphologies. SAXS was performed on the Advanced Polymers Beamline (X27C) at the National Synchrotron Light Source, Brookhaven National Laboratory, Upton, NY. The incident beam had an area of 3 mm^2 at the sample and a wavelength of 1.307 Å. The sample-to-detector

distance was 1.410 m. Two-dimensional scattering patterns were recorded on Fujitsu HR-V image plates and digitized using a Fujitsu BAS 2000 image plate reader. Background was subtracted, circular averaging was performed, and the data were converted to a logarithmic intensity scale for plots of log-(*I*) vs *q*.

Grain Structure Analysis. Quantitative estimates of grain size were obtained for the lamellar samples in this study (MG-4-5-36, MG-4-9-36, and MG-4-12-36) using procedures described by Garetz, Balsara, and co-workers.[16] TEM micrographs were digitized using an UMAX 1220S digitizer. The azimuthal angles, $\phi(\mathbf{r})$, which describe the local orientation of the lamellar normal at various points in the images, relative to a fixed reference direction, were computed by a local, two-dimensional Fourier analysis. Each image was divided into overlapping 245 nm × 245 nm squares with centers separated by 76.5 nm, and the image within this square was stored as a 32 × 32 element array of 8-bit integers. The correlation function, $C(r)$, was obtained using two models:

Model 1: $C(|\mathbf{r} - \mathbf{r}'|) \approx \langle\cos[2\{\phi(\mathbf{r}) - \phi(\mathbf{r}')\}]\rangle$. Random pairs of points, $\mathbf{r}$ and $\mathbf{r}'$, were chosen on a digitized micrograph, and the local Fourier transform analysis gave $\phi(\mathbf{r})$ and $\phi(\mathbf{r}')$. The ensemble averages, $\langle\cos[2\{\phi(\mathbf{r}) - \phi(\mathbf{r}')\}]\rangle$, were computed by repeating this procedure 10^6 times per micrograph. The distance scale, $r = |\mathbf{r} - \mathbf{r}'|$, was discretized into 76.5 nm interval bins. $C(|\mathbf{r} - \mathbf{r}'|)$ was determined for 12 images of MG-4-5-36, 13 images of MG-4-9-36, and 11 images of MG-4-12-36. For each sample, the correlation function was found by nonlinear regression to be approximately exponential with a baseline: $C(r) = \exp(-r/\kappa) + b$. The baseline values, b, were 0.041 (MG-4-5-36), 0.024 (MG-4-9-36), and 0.021 (MG-4-12-36).

Model 2: $C(|\mathbf{r} - \mathbf{r}'|)$ is the probability that both $\mathbf{r}$ and $\mathbf{r}'$ lie in the same grain. The correlation function was computed by choosing a random location, $\mathbf{r}$, on a digitized micrograph and computing $\phi(\mathbf{r})$. Then one travels along a random direction in the image examining $\phi(\mathbf{r}')$. The discretization of $r = |\mathbf{r} - \mathbf{r}'|$ and the images used here were the same as those used to compute $C(r)$ from model 1. If $|\phi(\mathbf{r}) - \phi(\mathbf{r}')|$ was less than a prescribed tolerance, $\Delta\phi$, then $\mathbf{r}$ and $\mathbf{r}'$ were considered to lie within the same grain and one was input in the corresponding bin, and $\mathbf{r}'$ was increased. When $\mathbf{r}' = \mathbf{r}^*$ was reached such that $|\phi(\mathbf{r}) - \phi(\mathbf{r}^*)| > \Delta\phi$, then zeros were input into all the remaining bins. This procedure was repeated 10^4 times for different $\mathbf{r}$ locations on each micrograph, and $C(r)$ was obtained by the averaging of these results. This method was used on the same 36 TEM micrographs as model 1. For each micrograph, the calculation was done for $\Delta\phi = 10°$, 15°, and 30°.

Photographic enlargements were made at different magnifications for each lamellar multigraft sample. A representative enlargement for sample MG-4-5-36 showed approximately 50 lamellar grains in an area of 100 μm^2. Each enlargement for sample MG-4-9-36 allowed examination of approximately 200 lamellar grains in an area of about 90 μm^2. Sample MG-4-12-36 was characterized using enlargements which showed an average of 30 μm^2 and approximately 400 grains each.

Grain size for the lamellar samples was also measured by a manual method. This provides a consistency check for the results obtained from the computerized image analysis. It also allows measurement of the grain shape anisotropy which could not be obtained by the current computer program. Photographic enlargements of the same TEM micrographs used for the computer analyses of grain size were overlaid with clear plastic sheets, and the outlines of grains were traced with a pen. The lamellar grains of the MG-4-n-36 samples are generally anisotropic. They are longer in the direction normal to the lamellae than parallel to the lamellae, consistent with previous results reported by Hashimoto and co-workers.[17,18] Additionally, within each micrograph the long axes of the grains approximately line up in the same directions. The transparent overlays of the grain outlines were oriented with the long axis of the grains along one principal direction and the short axis, orthogonal to the long axis, along the other. The overlays were digitally scanned and analyzed with a computer program that calculated the mean intercept lengths of test lines passed across the image in the two principal directions. These mean intercept lengths are proportional to, but not equal to, the actual average grain sizes in the two principal directions. The proportionality (constant of order one) between the mean intercept lengths and true average grain dimensions depends on the details of the grain shape.[19] Lacking a good model for grain shape, mean intercept lengths are taken as approximate indicators of grain size.

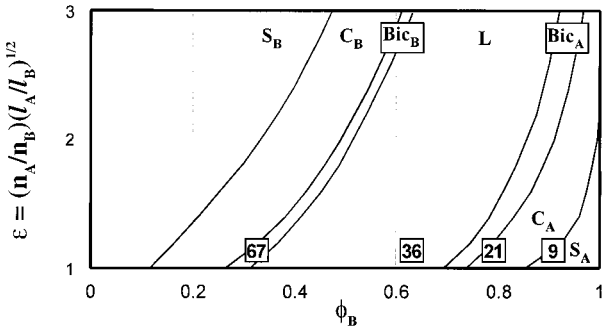

Figure 3. Morphology diagram generated by the Milner model for architecturally and conformationally asymmetric mixed arm stars of type A_nB_m having volume fraction ϕ_B and unified asymmetry parameter ϵ. In this study, PS is component A and PI is component B, such that $\epsilon \approx 1.2$. The four different volume fractions of samples considered in this work are placed on the diagram by their PI volume fraction but are labeled by their PS volume percent.

Results

To predict the morphological behavior of the regular multigrafts examined in this study, the morphological behavior for the appropriate constituting block copolymer was predicted using existing theory. For miktoarm star constituting block copolymers in the strong segregation limit ($\chi N > 100$), a theory derived by Milner models the effect of molecular architecture and composition on morphology.[8] For architecturally and conformationally asymmetric block copolymer stars of type A_nB_m, this theory predicts morphology as a function of component B volume fraction, ϕ_B, and a molecular asymmetry parameter, $\epsilon = (n_A/n_B)(l_A/l_B)^{1/2}$. Here, n_A and n_B are the numbers of arms of block materials A and B (n and m in the A_nB_m notation) linked at a junction point, and $l_i = V_i/R_i^2 = v_i/b_i^2$. V_i and R_i are the volume and radius of gyration of one arm of polymer i, while v_i is the segmental volume and b_i is the statistical segment length of component i. Figure 3 shows the morphology diagram, indicating a shift in the volume fraction ranges in which a given morphology is observed with increasing molecular asymmetry. The I_2S_2 constituting block copolymer has no architectural asymmetry because n_A and n_B are equal. The conformational asymmetry between PS and PI raises the total molecular asymmetry to $\epsilon \approx 1.2$.[20] In this case, PS is the A component and PI is the B component so that $\epsilon > 1$. The four volume fractions of the regular multigrafts in this study are located on the diagram at their volume fraction of PI but are labeled by their volume percent PS in keeping with previous block copolymer nomenclature. Using the Milner theory and the constituting block copolymer argument, the samples having 67 vol % PS are predicted to form cylinders of PI or possibly a bicontinuous morphology. The samples having 37 vol % PS are predicted to form lamellar morphologies. Those having 21 vol % PS are predicted to form cylinders of PS, and those having 9 vol % PS are predicted to form spheres of PS. Table 3 lists the predicted morphologies and

Table 3. Morphological Characterization Results for the 10 Regular, Tetrafunctional Multigrafts

sample	χN of constituting unit	predicted morphology	observed morphology	q^* (Å^{-1})	primary spacing (±5 Å)	lattice parameter (±5 Å)
MG-4-4-9	192	PS sp/PS cyl	dis/"mesh"	0.0252	249	
MG-4-8-9	192	PS sp/PS cyl	dis/"mesh"	0.0249	252	
MG-4-4-21	177	PS cyl	dis cyl	0.0211	297	
MG-4-7-21	177	PS cyl	dis Cyl	0.0218	288	
MG-4-9-21	177	PS cyl	dis Cyl	0.0225	279	
MG-4-5-36	161	lam	lam	0.0153	410	
MG-4-9-36	161	lam	lam	0.0177	354	
MG-4-12-36	161	lam	dis			
MG-4-10-67	113	PI cyl/bicont	PI cyl	0.0194	373	431
MG-4-14-67	113	PI cyl/bicont	PI cyl	0.0208	349	403

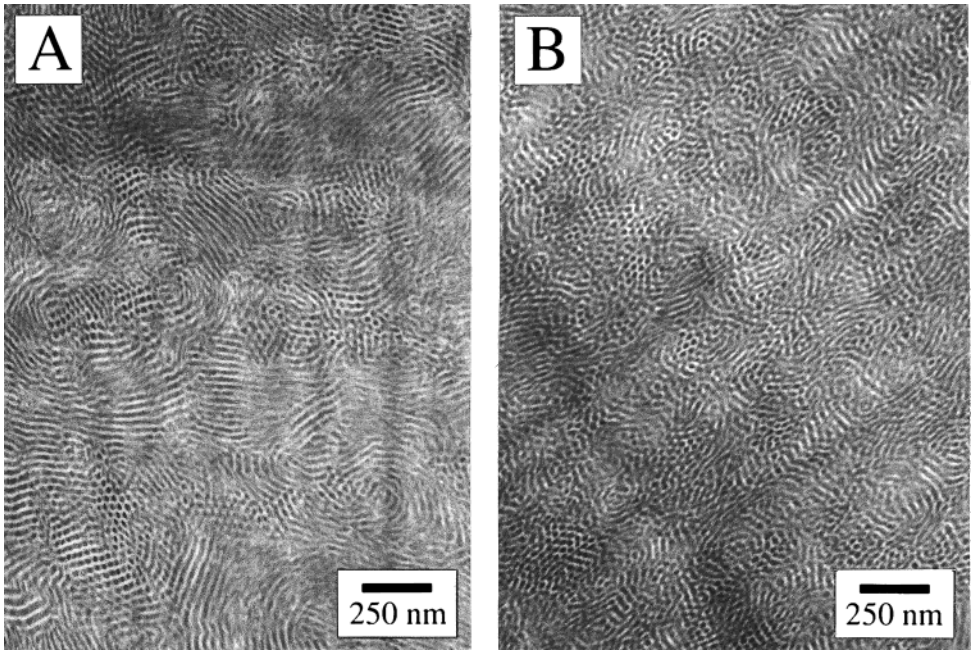

Figure 4. TEM micrographs for samples (a) MG-4-10-67 and (b) MG-4-14-67.

summarizes the results of the morphological characterization described below.

Figure 4 shows representative TEM micrographs from samples MG-4-10-67 (4a) and MG-4-14-67 (4b). These samples both have 67 vol % PS with on average 10 (MG-4-10-67) and 14 (MG-4-14-67) constituting block copolymer units per molecule. The morphology diagram in Figure 3 indicates that these samples are located at the cylinder/bicontinuous boundary. The representative TEM micrograph for MG-4-10-67, shown in Figure 4a, shows a cylindrical morphology. Figure 4b shows a slightly less well-ordered cylindrical morphology formed by MG-4-14-67. SAXS data for both samples, shown in Figure 5, exhibit strong primary reflections at q^* and higher-order reflections at $2q^*$ and $q^*\sqrt{7}$, consistent with hexagonally packed cylinders. The absence of the reflection expected for a hexagonal lattice at $q^*\sqrt{3}$ is due to a minimum in the cylindrical form factor. The SAXS data indicate that MG-4-10-67 has a (100) interplanar spacing of 373 Å and a hexagonal lattice parameter of 431 Å, while sample MG-4-14-67 has a (100) interplanar spacing of 349 Å and a hexagonal lattice parameter of 403 Å.

Samples MG-4-5-36, MG-4-9-36, and MG-4-12-36 were all predicted to form lamellar morphologies. As shown in Figure 6a, sample MG-4-4-36 exhibits a well-ordered lamellar morphology. SAXS data for this sample, shown in Figure 7a, exhibit four strong Bragg reflections at integral multiples of q^*. Sample MG-4-9-36 was found to have a lamellar but markedly less well-ordered

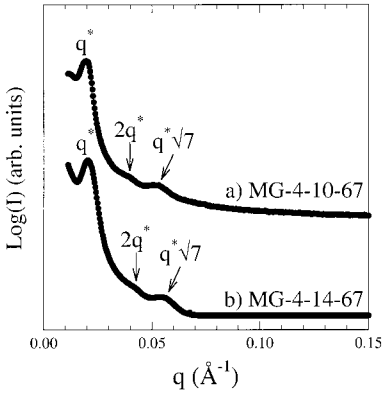

Figure 5. SAXS data for samples (a) MG-4-10-67 and (b) MG-4-14-67.

morphology. A representative TEM micrograph, shown in Figure 6b, shows smaller lamellar grains. SAXS data, shown in Figure 7b, still exhibit Bragg reflections at $2q^*$, $3q^*$, and $4q^*$, indicating a lamellar morphology, but their reduced intensities and increased width relative to the SAXS data for MG-4-5-36 result from the poorer ordering evident in Figure 6b. The morphology of sample MG-4-12-36, shown in Figure 6c, is microphase separated but generally not ordered on a lattice. A few very small regions that appear to be forming extremely small grains with some limited lamellar order are visible. Bragg reflections, indicative of well-developed order, are absent from the SAXS data for MG-4-12-36,

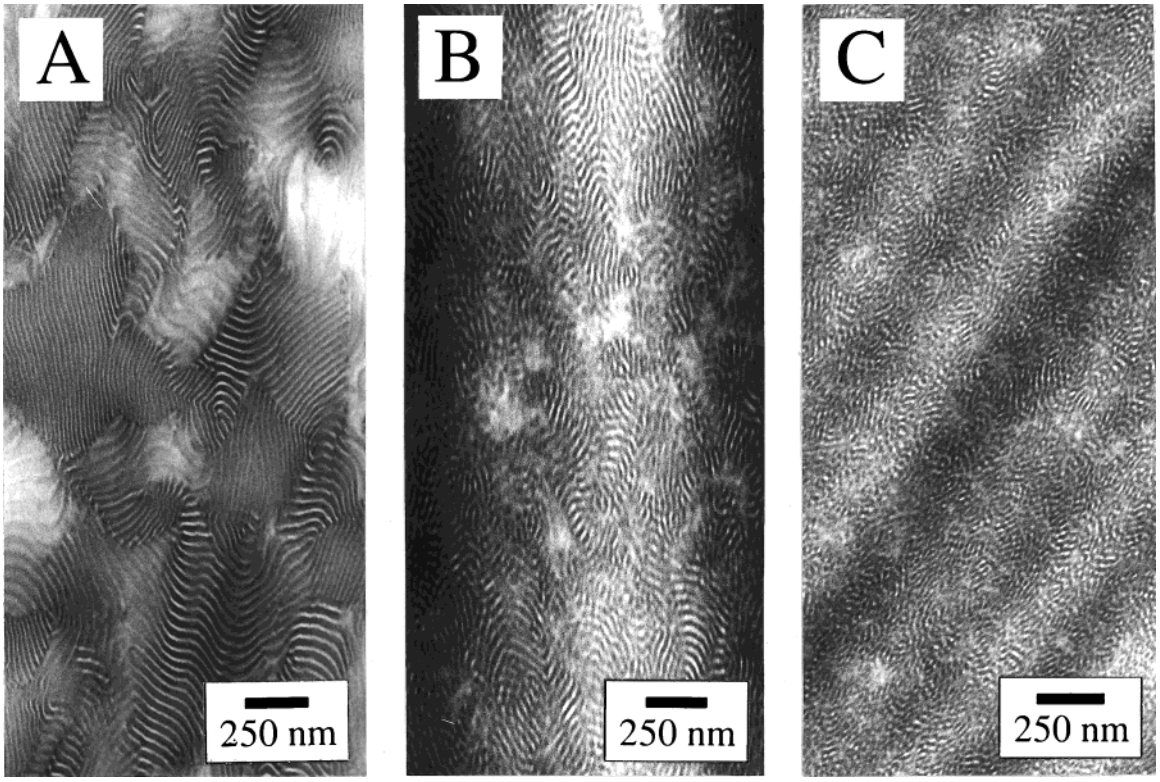

Figure 6. TEM micrographs for samples (a) MG-4-5-36, (b) MG-4-9-36, and (c) MG-4-12-36.

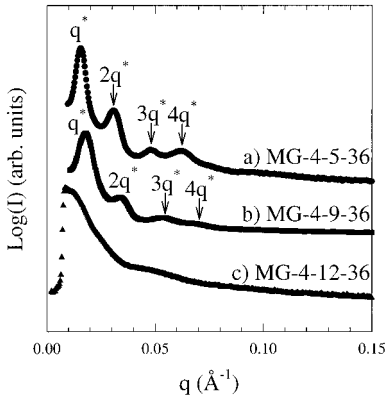

Figure 7. SAXS data for samples (a) MG-4-5-36, (b) MG-4-9-36, and (c) MG-4-12-36.

shown in Figure 7c. The lamellar spacings of MG-4-5-36 and MG-4-9-36 are 410 and 354 Å, respectively.

Figure 8 and Figure 9 show representative TEM micrographs and SAXS data, respectively, for the samples having 21 vol % PS: MG-4-4-21, MG-4-7-21, and MG-4-9-21. These samples were predicted to form cylindrical morphologies. As seen in Figure 8, each of these three samples formed a microphase-separated morphology which appears to lack long-range order. As was seen frequently in the study of random multigrafts,[7] the SAXS data for all samples in the MG-4-*n*-21 series exhibit a strong primary maximum followed by a weak, broad secondary maximum at approximately 2.5*q**, which does not correspond to a Bragg reflection for any known block copolymer morphology.[21] However, such scattering profiles are similar to intraparticle scattering which results from disordered arrangements of domains of a specific shape. Form factors for spheres and cylinders of the appropriate domain size were generated and compared to the scattering data. Domain sizes were obtained by using the primary peak to get an average center-to-center distance between neighboring domains. For samples MG-4-4-21, MG-4-7-21, and MG-4-9-21 these distances were found to be 297, 288, and 279 Å, respectively. This spacing along with the known PS and PI volume fraction can be used to calculate sphere and cylinder radii provided that a model for how the domains fill space is assumed. For the purposes of these calculations, cylinder radii were obtained assuming a hexagonal packing and sphere radii were determined using both bcc and sc lattice packings.[22,23] The use of lattices in these calculations is an approximation to allow calculation of domain size; it does not imply that that sample is actually ordered on a lattice. As in Figure 9 for MG-4-4-21, the form factors for spheres (both bcc and sc) fit the data poorly, predicting maxima where there are none, and extinctions coincident with the second maximum. Similar results, not shown, were obtained for MG-4-7-21 and MG-4-9-21. The form factor for a cylinder, however, fits the data better, with the form factor maximum corresponding with the observed secondary maximum. This suggests that the sample is composed of cylindrical, wormlike domains in a disordered arrangement. Similar calculations for samples MG-4-7-21 and MG-4-9-21 also support a preference for cylindrically shaped domains.

Samples MG-4-4-9 and MG-4-8-9 both formed the same unusual morphology, TEM images of which are given in Figure 10a,b. It may be described as a microphase-separated mesh of PS struts or wormlike domains in a PI matrix. SAXS data for samples MG-4-4-9 and MG-4-8-9, shown in Figure 11a,b, are consistent with a disordered, meshlike structure with average mesh sizes of 249 and 252 Å, respectively.

The SAXS and TEM data demonstrate that the domain shape of the graft copolymers is essentially independent of the number of constituting units, *n*.

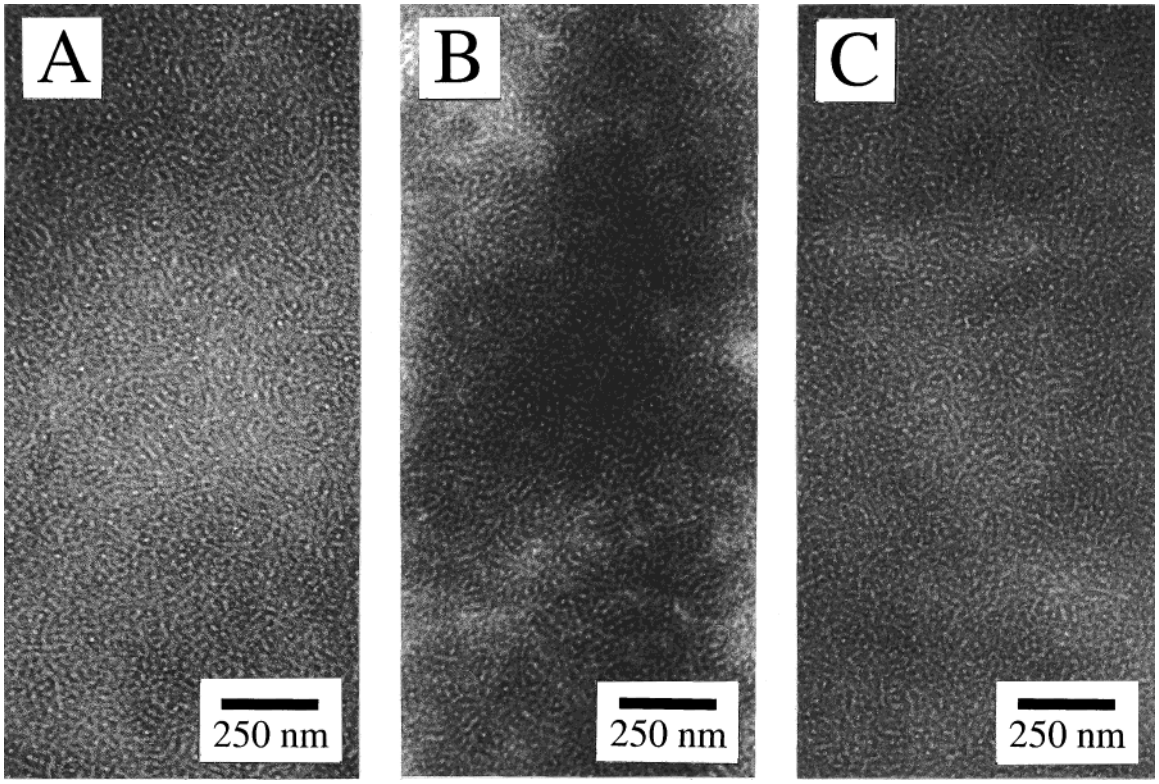

Figure 8. TEM micrographs for samples (a) MG-4-4-21, (b) MG-4-7-21, and (c) MG-4-9-21.

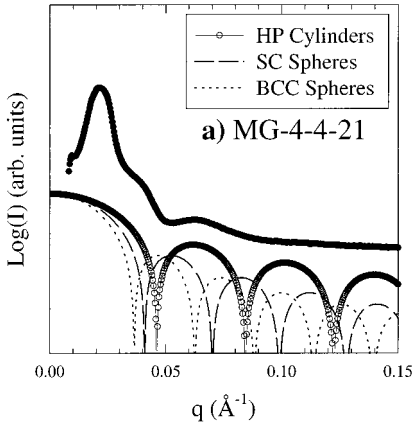

Figure 9. SAXS data for sample MG-4-4-21 with form factor profiles for hexagonally packed cylinders (open circles), sc spheres (dashed), and bcc spheres (dotted). Results for MG-4-7-21 and MG-4-9-21 are similar.

However, it is evident that increasing n decreases the coherent order or grain size of the microstructure. This is clearly visible in the three lamellar forming samples with PS volume fractions of 0.36. Figure 12 shows the correlation functions, $C(r)$, obtained using model 2 with a tolerance $\Delta\phi = 10°$ from three separate micrographs of MG-4-5-36. The results from the different micrographs are in reasonable agreement, and the correlation functions are exponentials to a good approximation: $C(r) = \exp(-r/\kappa)$, where κ is the correlation length. The lines in Figure 12 represent least-squares fits to this equation.

In Figure 13, the correlation functions from a single micrograph are presented using model 2 with different values of $\Delta\phi$. The correlation functions remain exponential, and as expected, the correlation length, κ, increases with increasing tolerance, $\Delta\phi$. Correlation functions for MG-4-5-36, MG-4-9-36, and MG-4-12-36, using model 2 with $\Delta\phi = 10°$, are shown in Figure 14. It is evident that κ decreases with increasing molecular weight; the long-range order in the samples is adversely affected by the increase in number of constituting block copolymer units. This trend is supported in Figure 15, where the correlation functions obtained from model 1 are plotted.

In Figure 16, the average values of κ, over all the TEM images analyzed, using the five methods outlined above (model 1, model 2 with different $\Delta\phi$ values, and manual), are plotted against n, the average number of junctions or constituting block copolymer units per molecule. The average grain size κ decreases with increasing n. The least-squares power law fit utilizing all of the data in Figure 16 (essentially averaging over all the different grain size measurement techniques) yields

$$\kappa \sim n^{-2.0} \tag{1}$$

The uncertainty in this power law exponent was estimated by looking at the range of exponents obtained by independent fits to the grain size data from the different measurement methods and was found to be ± 0.4.

Because the grain structure is anisotropic, the manual method gives two length scales: L_1 parallel to the lamellae and L_2 perpendicular to the lamellae. The grains are systematically larger perpendicular to the lamellae than parallel to the lamellae for all three samples. The ratio L_2/L_1 gives the aspect ratio of the grains, which is plotted in Figure 17 as a function of the number of junction points. The aspect ratio decreases from ~1.6 for MG-4-5-36 to ~1.1 for MG-4-12-36. Table 4 lists the grain size results for all samples studied and all the methods used.

Discussion

Of the 10 multigraft samples examined in this work, seven exhibited some degree of agreement with predic-

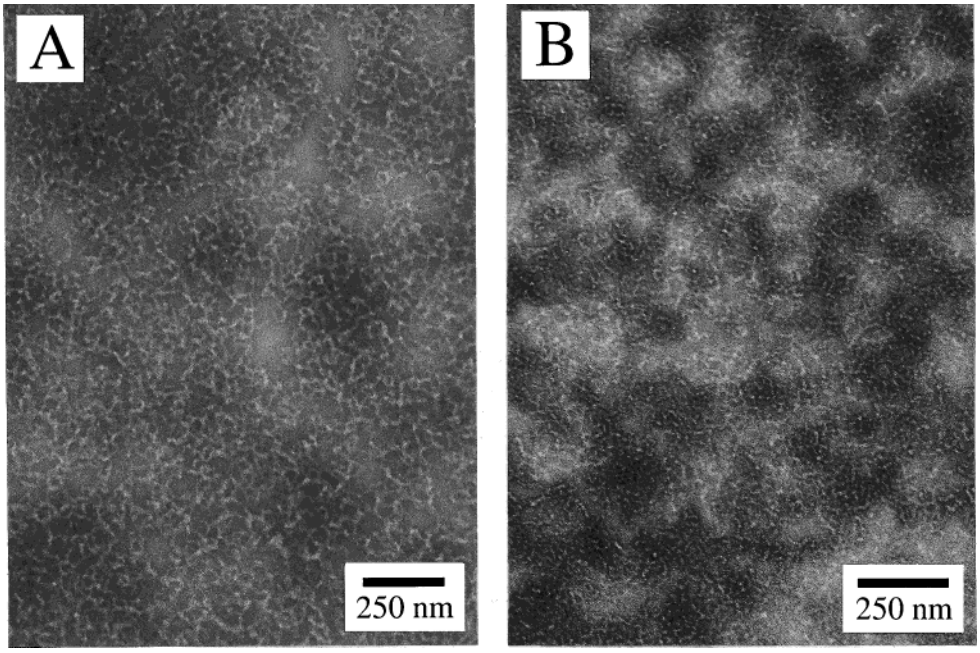

Figure 10. TEM micrographs for samples (a) MG-4-4-9 and (b) MG-4-8-9.

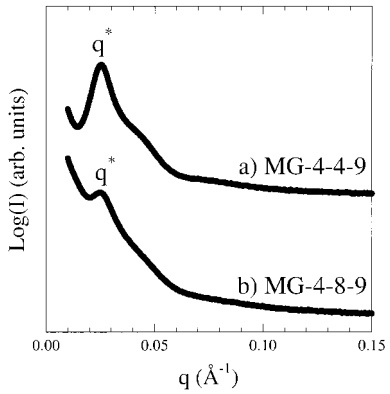

Figure 11. SAXS data for samples (a) MG-4-4-9 and (b) MG-4-8-9.

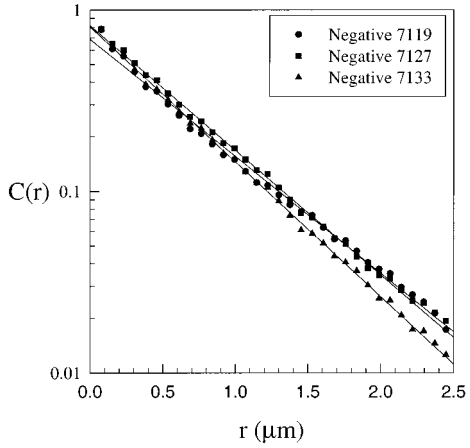

Figure 12. Correlation functions, $C(r)$, for MG-4-5-36 generated using model 2 with $\Delta\phi = 10°$ from three separate micrographs.

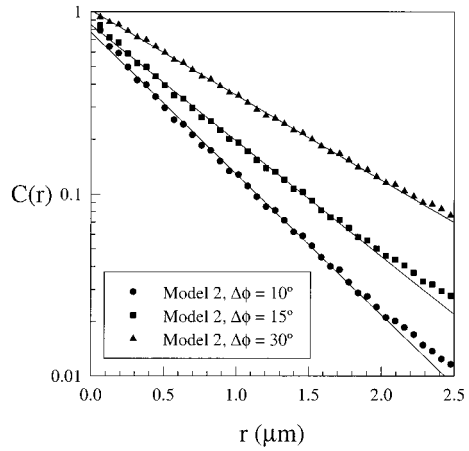

Figure 13. Correlation functions, $C(r)$, for MG-4-5-36 generated using model 2 with $\Delta\phi = 10°$, 15°, and 30°.

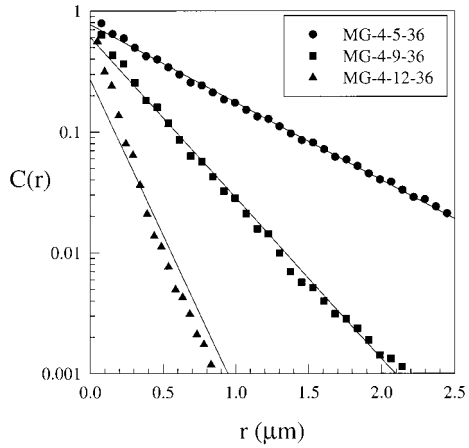

Figure 14. Correlation functions, $C(r)$, generated for MG-4-5-36, MG-4-9-36, and MG-4-12-36 using model 2 with $\Delta\phi = 10°$.

tions made by the constituting block copolymer hypothesis and the Milner theory (see Table 3). Samples of type MG-4-*n*-67 (hexagonal cylinders) and MG-4-*n*-36 (lamellae) formed the morphologies predicted by theory. Samples of type MG-4-*n*-21, which were predicted to form hexagonally packed cylinders, instead formed a microphase-separated structure of wormlike cylindrical domains without lattice ordering. This indicates that the preference for the theoretically predicted domain shape persists even as the long-range order is lost due

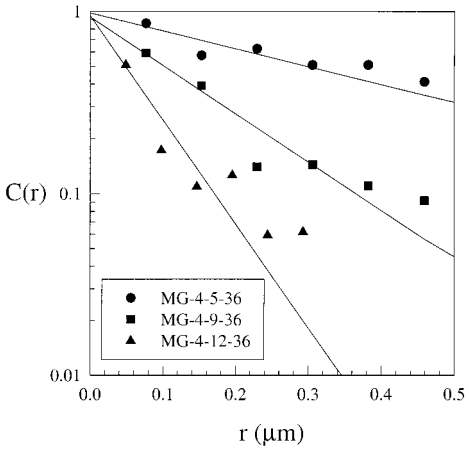

Figure 15. Correlation functions, $C(r)$, for MG-4-5-36, MG-4-9-36, and MG-4-12-36 generated using model 1.

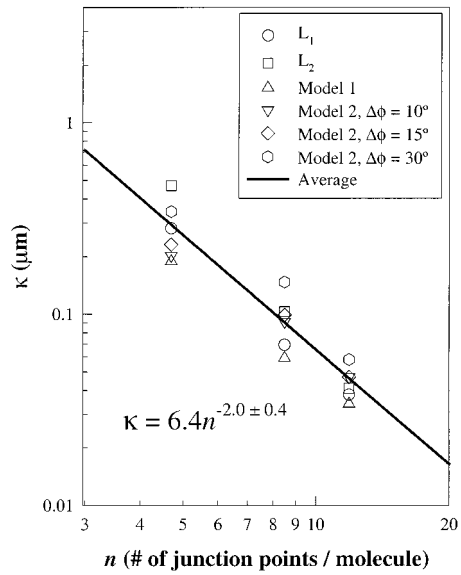

Figure 16. Power law fit to all correlation lengths (κ) and mean intercept lengths (L) for lamellar multigrafts MG-4-5-36, MG-4-9-36, and MG-4-12-36. κ is found to scale as $n^{-2.0}$, with an uncertainty in the exponent of ± 0.4.

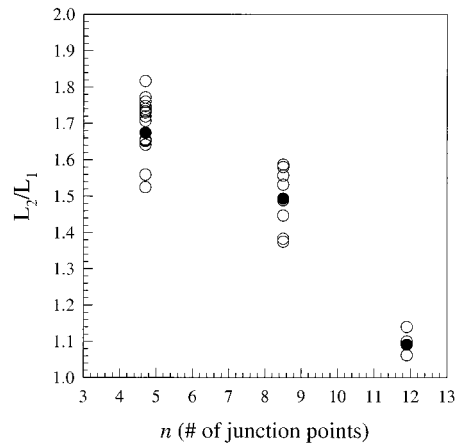

Figure 17. Lamellar grain aspect ratios (L_2/L_1), measured manually, given as a function of the number of junction points per molecule. Filled symbols are the average value for each sample.

presumably to decreased molecular mobility in these high molecular weight, multijunction point materials. The loss of lattice ordering before the loss of domain shape preference was also observed in the previous study of random multiple graft copolymers.[7] Only the MG-4-*n*-9 samples showed no agreement with theory at all, instead forming a microphase-separated mesh structure. This mesh, which looks like the early stages of spinodal decomposition although on a much smaller length scale, may result from a lack of molecular mobility in these materials with high molecular weight and many branch points.

Table 4. Summary of the Characteristic Length Scales (κ) and Mean Intercept Lengths (L) Collected Using Model 1, Model 2, and Manually

	model 1	model 2			manual method	
sample	κ (μm)	κ, $\Delta\phi = 10°$ (μm)	κ, $\Delta\phi = 15°$ (μm)	κ, $\Delta\phi = 30°$ (μm)	L_1 (μm)	L_2 (μm)
MG-4-5-36	0.189	0.202	0.231	0.344	0.281	0.469
MG-4-9-36	0.059	0.091	0.099	0.147	0.069	0.103
MG-4-12-36	0.034	0.047	0.047	0.058	0.038	0.041

The results of this study show that the constituting block copolymer hypothesis is self-consistent. In each of the four sets of samples based on four different constituting block copolymer units, all the fractions containing different average numbers of these units formed the same morphology. There was of course a progressive decrease in the degree of order in these structures with increasing number of constituting block units, but the structural similarities were clear. Also, within the lamellar (MG-4-*n*-36) and the two cylindrical (MG-4-*n*-67 and MG-4-*n*-21) sets of samples there was a noticeable decrease in the measured lattice constants or interdomain spacings with increasing *n*. Whether this is kinetic or thermodynamic in origin remains unclear.

The fact that the grain size of the lamellar MG-4-*n*-36 materials decreases with increasing number of junction points per molecule is to be expected. The fact that the grain shape anisotropy decreases with increasing number of junction points is perhaps less expected.

Conclusions

We have demonstrated the usefulness of the constituting block copolymer hypothesis to predict morphological behavior of the regular multigrafts. The self-consistency of the morphological behavior of molecules having the same constituting block copolymer confirms that the behavior of molecules with large, complex architectures is dictated by the behavior of the smaller architectural subunits from which they are comprised. The main effect of increasing the number of constituting block copolymer units per chain was to decrease the coherent order of the morphologies as measured by grain size.

The role of branch point location along the backbone can be examined by comparing the behavior of multigrafts with regularly located branch points to that of multigrafts with randomly located branch points.[7] In the study of multigrafts with random junction point placement, only lamellar morphologies formed any kind of long-range order. Cylindrical and spherical domain shapes formed but were not ordered on a lattice. Because of excluded-volume considerations, the lamellar domain shape templates its own long-range order to a much greater degree than spheres or cylinders.[7] The observation of limited lattice ordering in cylindrical samples in the regular multigraft series of this study indicates that regularity of graft placement improves

the ability of multiple-graft copolymers to form long-range order. This is most likely a thermodynamic, rather than a kinetic, effect because both the random and regular multigraft materials had similar molecular weights and similar numbers of branch points per molecule. The multigraft materials with random junction point locations are frustrated due to the fact that different regions of the molecule want to form different morphologies due to the fluctuating local junction point density.[24] This undoubtedly suppresses the driving force for the formation of the structure based on the average constituting block copolymer over the case of the regular multigrafts, where every local region of every molecule wants to do exactly the same thing. Note that the random multigraft materials actually have lower overall polydispersities than the fractionated regular multigrafts. Clearly then it is the regularity of the local molecular architecture per junction point, rather then the overall polydispersity, that has the greater effect on long-range order.

Acknowledgment. Work at the University of Massachusetts was funded by the U.S. Army Research Office under Contracts DAAG55-98-1-0116 and DAAG55-98-1-0005. Funding from the ARO for the purchase of the MALDI (DAAG55-97-1-0075) is gratefully acknowledged, as is funding from the National Science Foundation supporting the purchase of the Waters Alliance SEC (DMR-9802853). Central Facility support from the Materials Research Science and Engineering Center (MRSEC) at the University of Massachusetts—Amherst as well as the W. M. Keck Electron Microscopy Laboratory is also acknowledged. Work at Polytechnic University was supported by the National Science Foundation (DMR 9901951), the Dreyfus Foundation, and the Petroleum Research Fund, administered by the American Chemical Society. Yunan Wan, Lujia Bu, Haining Ji, and Kunlun Hong are acknowledged for significant contributions to the molecular characterization.

References and Notes

(1) Noshay, A.; McGrath, J. E. *Block Copolymers: Overview and Critical Survey*; Academic Press: New York, 1977.
(2) Xenidou, M.; Hadjichristidis, N. *Macromolecules* **1998**, *31*, 5690.
(3) Iatrou, H.; Mays, J. W.; Hadjichristidis, N. *Macromolecules* **1998**, *31*, 6697.
(4) Gido, S. P.; Lee, C.; Pochan, D. J.; Pispas, S.; Mays, J. W.; Hadjichristidis, N. *Macromolecules* **1996**, *29*, 7022.
(5) Lee, C.; Gido, S. P.; Poulos, Y.; Hadjichristidis, N.; Beck Tan, N.; Trevino, S. F.; Mays, J. W. *Polymer* **1998**, *39*, 4631.
(6) Lee, C.; Gido, S. P.; Poulos, Y.; Hadjichristidis, N.; Beck Tan, N.; Trevino, S. F.; Mays, J. W. *J. Chem. Phys.* **1997**, *107*, 6460.
(7) Xenidou, M.; Beyer, F. L.; Gido, S. P.; Hadjichristidis, N.; Beck Tan, N. *Macromolecules* **1998**, *31*, 7659.
(8) Milner, S. T. *Macromolecules* **1994**, *27*, 2333.
(9) Olmsted, P. D.; Milner, S. T. *Macromolecules* **1998**, *31*, 4011.
(10) Whitmore, M. D.; Vavasour, J. D. *Acta Polym.* **1995**, *46*, 341.
(11) Vavasour, J. D.; Whitmore, M. D. *Macromolecules* **1993**, *26*, 7070.
(12) Benoit, H.; Hadziioannou, G. *Macromolecules* **1988**, *21*, 1449.
(13) Shinozaki, A.; Jasnow, D.; Balazs, A. C. *Macromolecules* **1994**, *27*, 2496.
(14) Olvera de la Cruz, M.; Sanchez, I. C. *Macromolecules* **1986**, *19*, 2501.
(15) Cowie, J. M. G. In *Developments in Block Copolymers - 1*; Goodman, I., Ed.; Applied Science Publishers: New York, 1982; p 1.
(16) Garetz, B. A.; Balsara, N. P.; Dai, H. J.; Wang, Z.; Newstein, M. C.; Majumdar, B. *Macromolecules* **1996**, *29*, 4675.
(17) Hashimoto, T.; Sakamoto, N.; Koga, T. *Phys. Rev. E.* **1996**, *54*, 5832.
(18) Sakamoto, N.; Hashimoto, T. *Macromolecules* **1998**, *31*, 3815.
(19) Underwood, E. E. *Quantitative Stereology*; Addison-Wesley Publishing Company: Reading, MA, 1970.
(20) Pochan, D. J.; Gido, S. P.; Pispas, S.; Mays, J. W.; Ryan, A. J.; Fairclough, J. P. A.; Hamley, I. W.; Terrill, N. *Macromolecules* **1996**, *29*, 5091.
(21) Skoulios, A. E. In *Developments on Block Copolymers - 1*; Goodman, I., Ed.; Applied Science Publishers: New York, 1982; p 81.
(22) Oster, G.; Riley, D. P. *Acta Crystallogr.* **1952**, *5*, 1.
(23) Oster, G.; Riley, D. P. *Acta Crystyllogr.* **1952**, *5*, 272.
(24) Qi, S.; Chakraborty, A. K.; Wang, H.; Lefebvre, A. A.; Balsara, N. P.; Shakhnovich, E. I.; Xenidou, M.; Hadjichristidis, N. *Phys. Rev. Lett.* **1999**, *82*, 2896.

MA991141S